J Mater Sci (2017) 52:5807–5821

L-cysteine-reduced graphene oxide/poly(vinyl alcohol) ultralight aerogel as a broad-spectrum adsorbent for anionic and cationic dyes

Jianliang Xiao[1], Weiyang Lv[1], Zhou Xie[1], Yihu Song[1,*], and Qiang Zheng[1]

[1] *MOE Key Laboratory of Macromolecular Synthesis and Functionalization, Department of Polymer Science and Engineering, Zhejiang University, Hangzhou 310027, China*

Received: 1 December 2016
Accepted: 17 January 2017
Published online: 20 January 2017

ABSTRACT

It is a challenge to develop broad-spectrum, high-efficiency, easy-recyclable adsorbents for the removal of water contaminants. Herein, *L*-cysteine-reduced graphene oxide/poly(vinyl alcohol) (CRG/PVA) ultralight aerogels with good mechanical strength and reusability are prepared via a direct sol–aerogel transition strategy by freeze drying. At optimized composition, the aerogel shows high adsorption efficiency toward both cationic and anionic dyes, overcoming the defect of many traditional adsorbents that usually can only remove one type of organic dyes. The adsorption is proved to involve in π–π interaction between CRG and dyes, endowing the aerogel with universality in adsorbing a wide range of conjugated dyes. Moreover, a remarkable synergetic effect is observed for removal of two oppositely charged dyes from aqueous system, yielding exceptionally high total adsorption capacities surpassing all known adsorbents examined for removing binary dyes. Thus, the CRG/PVA aerogel demonstrates great potential for usage as reusable, high-efficiency, and broad-spectrum adsorbent in water treatment.

Introduction

Water contamination as an outgrowth of the rise of manufacturing industry becomes more and more conspicuous [1]. Organic dye widely used in textiles, paper, coatings, and leather is one of the main contaminants in water, causing a serious environmental threat to aquatic and human life [2]. Approximately over 7×10^5 tonnes per year of dyes is discharged into the water bodies all over the world [3]. Dyes in water are mainly cationic and anionic, and both can cause severe problems to aquatic environment [4]. Various practices have been employed for the treatment of dye-bearing wastewater [5], among which adsorption proves to be one of the most versatile methods due to its relatively high efficiency, simple design, convenient operation, and no secondary pollution [6, 7]. However, traditional absorbents such as polymer nanoparticle [8], nanofiber [9], activated carbon [10], layered double hydroxide [11], clays [12],

Address correspondence to E-mail: s_yh0411@zju.edu.cn

DOI 10.1007/s10853-017-0818-y

and multi-walled carbon nanotubes [13] suffer from the limitation of adsorption capacity, efficiency, and recycling ability [9].

Recently, graphene and its derivatives with theoretical specific surface area as large as 2620 m^2/g have been frequently reported as high-capability absorbents toward organic dyes [2, 14–19]. However, the trend to aggregate and difficulties in separation and recycling of two-dimensional graphene adsorbents vastly limit the applications [20, 21]. Thus, three-dimensional graphene-based porous materials are attracting more and more attention due to their large specific surface area and good recyclability [21–24]. For example, graphene oxide (GO) sponge prepared by centrifugal vacuum evaporation method is able to remove methylene blue (MB) and methyl violet with adsorption capacities of 397 and 467 mg/g, respectively [25]. Polydopamine-functionalized graphene hydrogels via hydrothermal self-assembly method is able to remove rhodamine B and *p*-nitrophenol [26]. However, the GO sponge could not keep stable shape due to the severe hydroscopicity [25], and the functionalized graphene hydrogels are too fragile to handle [22]. More seriously, the adsorption capability is usually not high enough due to sacrifice of specific surface area resulted from nanosheet self-assembly and π–π stacking. The introduction of a polymer acting as both promoter for gelling and protector from over-aggregation is excepted to solve these problems [23]. Sui et al. [27] prepared GO/polyethylenimine porous materials exhibiting high adsorption capability toward anionic dyes amaranth and orange. Xu et al. [28] prepared a GO/DNA hydrogel with impressive environmental stability, mechanical property, and high adsorption efficiency for cationic safranine O. Unfortunately, these materials can only remove one type of dye (anionic or cationic). Thus, preparation of high-efficiency and broad-spectrum adsorbents remains still a challenge.

Generally, electrostatic and π–π interactions are responsible for removal of aromatically structured ionic dyes by graphene-based adsorbents [25, 29]. However, the electrostatic attraction is adverse for broad-spectrum adsorption given that it is applicative only to oppositely charged dyes. Thus, the negatively charged GO shows high adsorption capability toward cationic dyes [25] rather than anionic dyes [20, 30]. On the other hand, the strong π–π interaction between aromatically structured dyes and graphene could endow materials with broad-spectrum adsorption capability being independent of charges. Nevertheless, enhancing π–π interaction by improving structural conjugacy usually brings risks of graphene aggregating and even restacking [31], which greatly reduces the specific surface area and adsorption capability of adsorbents. Thus, protecting graphene from over-stacking is vital in acquiring high-capability, broad-spectrum adsorptivity.

Preparing broad-spectrum, high-capability, reusable graphene-based adsorbents requires non-stacked graphene nanosheets to form a perfect network with good mechanical strength and swelling resistance. We in a previous article reported that L-cysteine-reduced graphene oxide (CRG) possesses good conjugate structure and dispersity in aqueous solution and exhibits high adsorption efficiency toward anionic, nonionic and cationic dyes [32]. However, an inevitable defect that a centrifugation or filtration step is necessary to separate the adsorbent from solution brings much limitation in practical applications. We herein develop a CRG/poly(vinyl alcohol) (CRG/PVA) porous aerogel to endow the material with good mechanical strength and excellent swell resistance and reusability. PVA is introduced for stabilizing CRG nanosheets, avoiding stacking and providing with good elasticity and strength. Due to the π–π interaction between CRG and dye molecules, the aerogel shows super adsorption capability toward cationic neutral red (NR), anionic indigo carmine (IC) and several other dyes, demonstrating great potential to be used as a broad-spectrum, high-capability and reusable adsorbent for water treatment.

Materials and methods

Materials

Graphite (99.8%, average particle size 45 μm) and L-cysteine were obtained from Alfa (UK). Poly(vinyl alcohol) (PVA, weight-averaged molecular weight 75,000–79,000, 99% hydrolyzed) was purchased from Sinopharm Chem. Reagent Co. Ltd., China. Concentrated sulfuric acid (H_2SO_4) and hydrochloric acid (HCl), phosphorus pentoxide (P_2O_5), potassium persulfate ($K_2S_2O_8$), hydrogen peroxide (H_2O_2, 30%), potassium permanganate ($KMnO_4$), sodium hydroxide (NaOH), neutral red (NR), indigo carmine (IC), and other dyestuffs were purchased from Aladdin

(China). All the materials were used without purification.

Preparation of CRG/PVA aerogels

GO prepared from graphite by a modified Hummer's method [33] was used to synthesize CRG [32]. In brief, GO (50 mg) was suspended in deionized water (100 mL) and L-cysteine (500 mg) was added under stirring. After reaction for 48 h at room temperature (~25 °C), the product was centrifuged at 14,000 rpm. The collected product was washed with 0.1 M NaOH solution to remove residual L-cysteine, followed by repeated washing with deionized water until pH of the supernatant reached 7.0. The PVA solutions were prepared by stirring PVA solid in deionized water at 90 °C for 3 h until completely dissolved. The CRG/PVA suspensions were obtained by mixing CRG suspensions (1%) and PVA solutions (2%) with different ratios and diluting to different initial concentrations. Then, the suspensions were frozen at −30 °C for 12 h and freeze-dried at −50 °C for 48 h to CRG/PVA aerogels.

Batch adsorption experiments

Batch adsorption experiments were conducted by adding 5 mg aerogel into 15 mL dye solutions (20 mL for adsorption of dye mixture). After equilibration under vibration at 30 °C, the supernatant was analyzed using UV–Vis absorbance spectra according to a pre-established calibration curve to determine dye content. The dye removal efficiency (E_r) and equilibrium adsorption amount (q_e) were calculated according to

$$E_r = 100(1 - C_e/C_0) \quad (1)$$

$$q_e = V(C_0 - C_e)/m \quad (2)$$

where C_e and C_0 are equilibrium and initial dye concentrations of the solution, respectively, V is volume of dye solution, and m is weight of aerogel.

Characterization

Atomic force microscope (AFM, Bruker-Dimension Edge, USA) and scanning electron microscope (SEM, S4800, Hitachi, Japan) were used to observe the morphology of nanosheets and aerogels. Thermal stability of aerogels was evaluated by thermogravimetric analyzer (TGA, Q1000, TA, USA) at a heating rate of 10 °C min^{-1} under nitrogen. Raman spectra were collected on a Raman spectrometer (Almega-Dispersive, Thermo Nicolet, USA) with a 514.5 nm excitation. UV–Vis absorption spectra were measured on a UV–Vis spectrophotometer (CARY100, Varian, USA). X-ray diffraction (XRD) was carried out on a diffractometer equipped with Cu Kα radiation ($\lambda = 0.154$ nm) (Rigaku D/max 2550, Shimadzu, Japan). Fourier transform infrared (FTIR) spectra were collected on a spectrometer (Vector 22, Bruker Optics, USA). Specific surface area was calculated based on N_2 absorption isotherm measured with an Autosorb-1-c system (Quantachrome, USA).

Results and discussion

Morphology and structure of aerogels

Preparation of aerogels normally involves three steps: sol–gel transition (gelation), network perfection (aging), and gel–aerogel transition (drying) [23]. All the three steps could affect the microstructure, properties and applications of aerogels. Here we develop a direct sol–aerogel transition protocol (Scheme 1). Semi-crystalline PVA that strongly interacts with nanoparticles via hydrogen bonding [34–37] is chosen to incorporate with CRG, and the aerogels are directly made from the fluid suspension, tremendously simplifying the process.

GO can be easily exfoliated into sheets of 1.1 nm in thickness and more than 10 μm in lateral size (Fig. 1a), being the typical character of single-layer GO sheet [38]. After reduction, CRG sheet is still single-layered, with an average thickness of 0.4 nm and a width less than 5 μm due to the elimination of functional groups (Fig. 1b). The effective reduction is further confirmed by TGA, Raman and UV–Vis spectra, as shown in Online Resource 1 (Fig. S1). The large lateral size endows CRG nanosheets with ability to self-assembly into three-dimensional structure during freezing drying via π–π stacking [39], while the residual carboxyl groups at the edge of the nanosheets make it possible to stably disperse CRG in PVA aqueous solution [32].

Stable PVA aerogels physically cross-linked by crystallites or PVA-based composite aerogels can be prepared by freeze drying from aqueous PVA solutions [36, 40–47]. Figure 1c shows morphology of PVA aerogels obtained by freeze drying from a

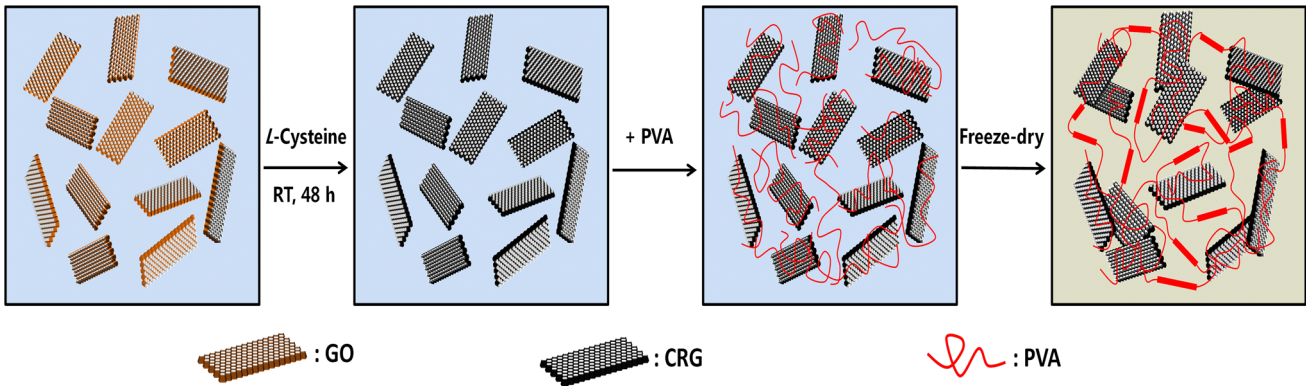

Scheme 1 Illustration of the preparation process of the CRG/PVA aerogels.

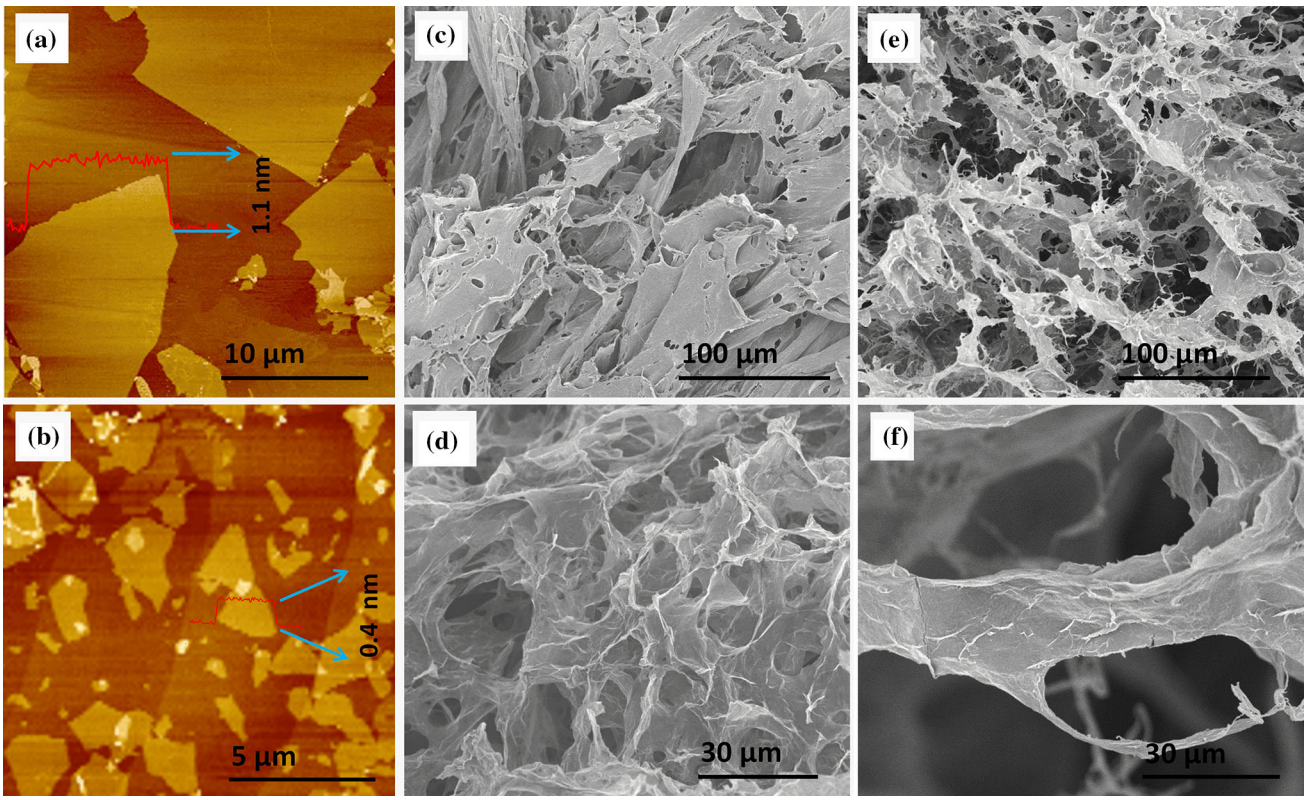

Figure 1 AFM images of GO (**a**) and CRG (**b**) deposited on mica sheet and SEM images of PVA (**c**), CRG (**d**), and CRG/PVA (**e**, **f**) aerogels.

0.5 wt% solution. However, the pore size of this aerogel is non-uniform, and the walls of pores are pretty thick, giving rise to a small specific surface (6.7 m^2/g, Fig. S2a in Online Resource 1). On the other hand, pure CRG aerogel obtained by the same method from a 0.25 wt% suspension has a well-defined and interconnected porous network with thin walls of pore (Fig. 1d). However, self-assembly of CRG nanosheets vastly reduces the specific surface area (175.6 m^2/g, Fig. S2b in Online Resource 1) of the porous CRG aerogels. PVA macromolecules could stabilize CRG in the dispersion via interfacial hydrogen bonding [37], thus avoiding excessive aggregation of nanosheets during aerogel formation and yielding the CRG/PVA aerogel (from 0.25%/0.5% suspension) with pore size being larger than the CRG aerogel and more uniform than the PVA aerogel (Fig. 1e, f). This composite aerogel owns a specific

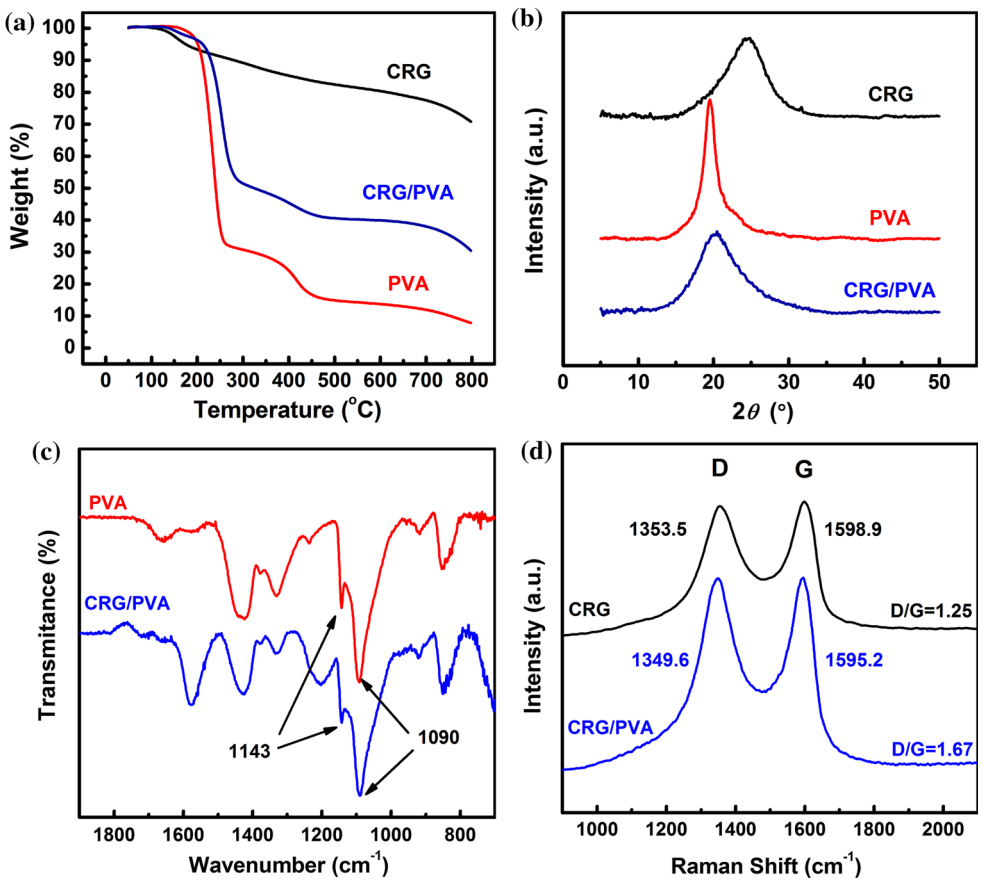

Figure 2 TGA curves (**a**), XRD (**b**), FTIR (**c**), and Raman (**d**) spectra of CRG (C_0 = 0.25 wt%), PVA (C_0 = 0.5 wt%), and CRG/PVA (C_0 = 0.25 wt%/0.5 wt%) aerogels.

surface area of 182.6 m^2/g (Fig. S2c in Online Resource 1), being higher than those of pure CRG and PVA aerogels. Considering the little mass fraction of CRG during the aerogel preparation, it is evident that PVA chains can effectively prevent excessive aggregation of nanosheets and increase the specific surface area.

The thermal stability of aerogels is investigated, as shown in Fig. 2a. The CRG aerogel exhibits about 30% weight loss resulted from removal of the remained oxygen-containing functional groups [48]. The PVA aerogel decomposes in two steps, *i.e.*, hydroxyl dehydration (200–350 °C) and carbon chain decomposition (400–500 °C) [49]. It is interesting that the CRG/PVA aerogel exhibits thermal decomposition temperatures higher than that of PVA aerogel. The peak temperature of derivative thermogravimetric curve corresponding to the maximum weight loss rate is 17.5 °C higher than the PVA aerogel (Fig. S3 in Online Resource 1). The significantly improved thermal stability of the CRG/PVA aerogel might be attributed to the high chain compactness due to the interaction (*i.e.*, hydrogen bonding) between PVA chains and well-aligned nanosheets [37].

Figure 2b shows XRD spectra of aerogels. The CRG aerogel exhibits a weak diffraction at $2\theta = 23.2$ °, corresponding to a *d*-spacing of 0.39 nm [50]. This characteristic peak disappears in the CRG/PVA aerogel, indicating a good exfoliation of CRG nanosheets [51]. Moreover, the diffraction peak of crystalline PVA at $2\theta = 19.5$ ° becomes weaker and broader in the CRG/PVA aerogel, which might be assigned to the PVA/CRG interfacial interactions that decrease the PVA interchain interaction and lower crystallinity [52]. The same result is also reflected by FTIR spectra (Fig. 2c). The peak at 1143 cm^{-1} in the spectra of PVA is assigned to symmetric C–C stretching mode of a portion of chain where an intramolecular hydrogen bond is formed between two neighboring -OH groups located on the same side of the plane of the PVA carbon chain [53]. Its intensity is influenced by the crystalline portion of the chains. The peak at 1090 cm^{-1}, whose intensity is constant in all samples, is used as an inner reference.

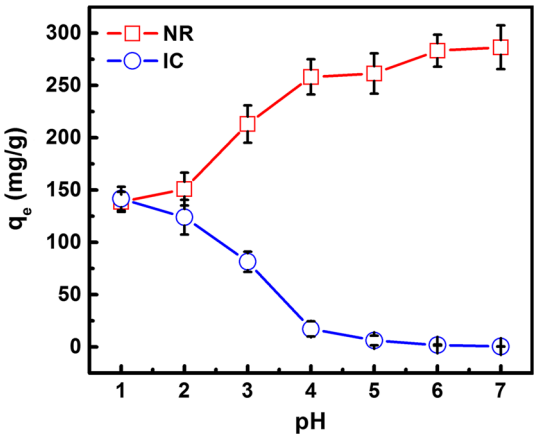

Figure 3 Effects of pH on q_e of NR (*squares*) and IC (*circles*).

The intensity of the 1143 cm^{-1} peak normalized by that of the 1090 cm^{-1} peak decreases in the CRG/PVA aerogel in comparison with the PVA aerogel, which could be assigned to reduced crystallinity in the composite aerogel. The interaction between CRG and PVA was further investigated by Raman spectra, as shown in Fig. 2d. The CRG aerogel displays a D band at 1353.5 cm^{-1} and a G band at 1598.9 cm^{-1}, attributed to the first-order scattering of E2 g mode [54] and the reduced size of the in-plane sp^2 domains [55], respectively. After complexation with PVA, the D and G bands shift to lower wavenumbers and the intensity ratio of D to G band increases, which is ascribed to the delocalized π-electrons and increased disorder of CRG nanosheet interacting with PVA chains [56]. In brief, the hydrogen bonding between the residual oxygen-containing groups on CRG nanosheets and -OH groups on PVA chains results in the adsorption and immobilization of a portion of PVA chains, which prevents CRG nanosheets from stacking and reduces crystallinity of PVA, yielding the aerogel with considerably large specific surface area.

Effect of pH on adsorption

The reduction reaction by L-cysteine mainly removes epoxy/hydroxyl groups, and most of carboxyl groups at the edge of the nanosheet remain [32, 57]. Thus, pH of solution tremendously affects the surface charge and adsorption capacity of CRG/PVA aerogels toward ionic dyes [4]. The effect of pH on the adsorption is shown in Fig. 3. NR is positively charged [58] in aqueous solution at higher pH; thus, the negatively charged surface of CRG in the CRG/PVA aerogels due to ionization of residual carboxyl groups favors the absorption of NR [59] through electrostatic attraction, resulting in a higher q_e. To the contrary, the repulsion between anionized sulfonyl of IC and carboxyl group of CRG in the CRG/PVA aerogels lowers the adsorption capacity of IC. At lower pH value, the repulsion between CRG and IC is shielded, yielding a higher q_e of IC. In brief, the CRG/PVA aerogels exhibit high adsorption efficiencies for NR and IC at high and low pH values, respectively. At low pH where the electrostatic interaction is shielded, the q_e values of NR and IC are comparative to each other, indicating that the adsorptions of both dyes share the same mechanism in this case. Taking practical applications into account, unless declared otherwise in following experiments, pH values of 7 and 2 are used for NR and IC solutions, respectively.

Effect of composition on adsorption

PVA chains are able to effectively segregate CRG nanosheets to avoid over-stacking and provide mechanical strength, while the adsorption performance is mostly rooted in CRG [32]. Therefore, the concentrations of both PVA and CRG in the dispersions are quite important for the formation and adsorption performance of the resultant aerogels. In general, lower dispersion concentrations bring lower aerogels density and higher water absorbency (Fig. 4a and Fig. S4), except for samples made from the 0.15%/0.15% (CRG/PVA) and 0.15%/0.30% (CRG/PVA) dispersions. These two aerogels shrink during drying (Fig. 4d), giving rise to slightly higher densities and lower water absorbency. The CRG/PVA aerogels are ultralight, with densities varying from 7.3 to 14.4 mg/cm^3.

The mass fraction of CRG is another factor determining the aerogels performance. Given that CRG is mainly responsible for the adsorption capability, higher mass fraction of CRG favors the adsorption. For example, the 0.50%/0.50% and 0.15%/0.15% aerogels own the highest q_e, while the 0.25%/1.0% one has the lowest (Fig. 4b). However, taking the use efficiency of CRG (q_e per CRG mass, q_e/CRG) into consideration, CRG in the 0.25%/1.0% aerogel exhibits the highest adsorption capability (Fig. 4c). Of cause, very high fraction of CRG sacrifices the use efficiency and raises up the cost. It is interesting that, at the same CRG concentration in the dispersions,

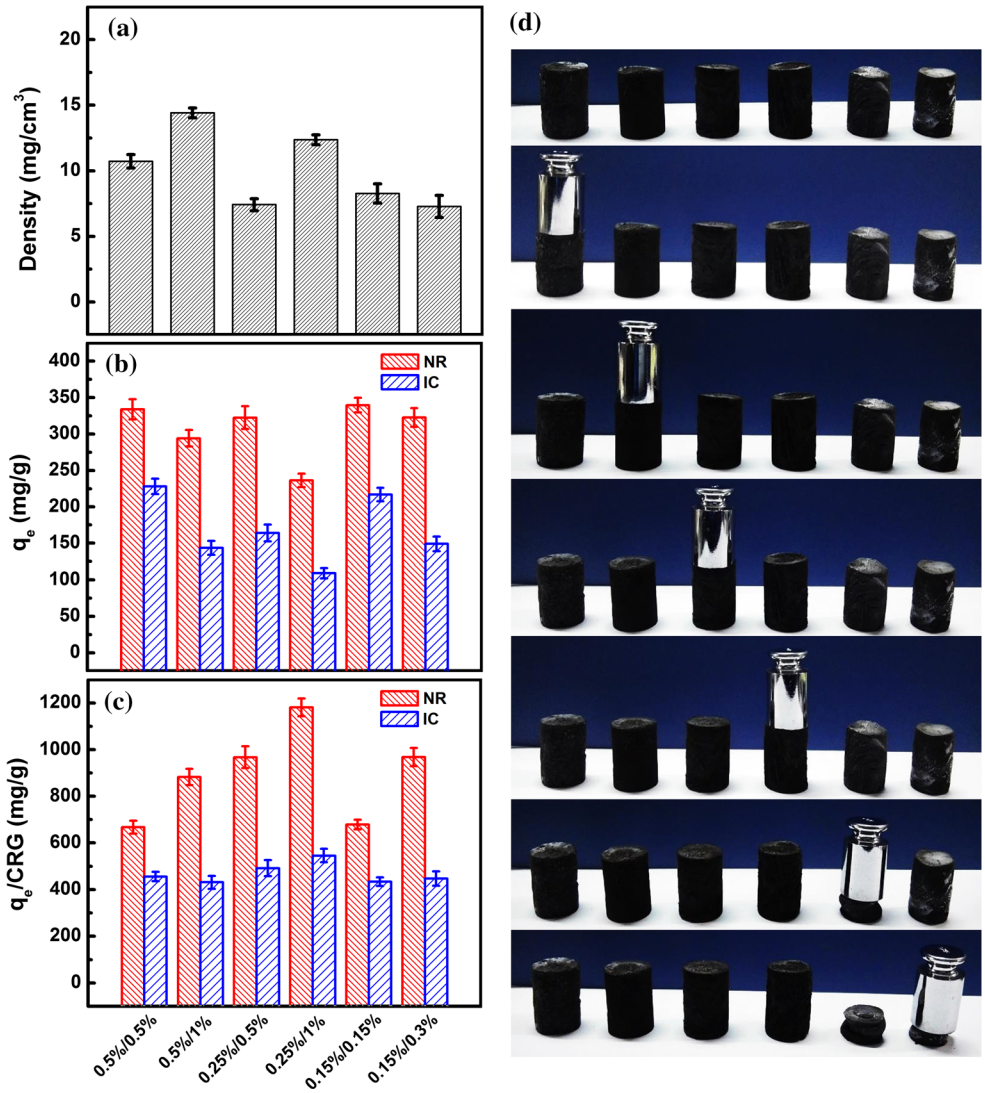

Figure 4 Apparent density (**a**), q_e toward NR and IC at $C_0 = 150$ mg/L (**b**), q_e per CRG mass (**c**), and optical images (**d**) of aerogels prepared from suspensions with different initial concentrations of CRG and PVA. Each aerogel is identified in the form of CRG (wt%)/PVA (wt%), and all graphs share the same left-to-right order of samples.

increasing PVA content facilitates the adsorption efficiency of CRG, evidencing that PVA could effectively prevent CRG from aggregation. At the same mass fraction of CRG, the adsorption capabilities of aerogels prepared from different initial concentrations follow the opposite trend of densities. The lower density favors the adsorption performance of aerogels, which might be ascribed to the higher water absorbency (Fig. S4 in Online Resource 1).

The mechanical properties of aerogels depend on the composition too (Fig. 4d). Due to introduction of PVA that brings toughness and strength, most of the CRG/PVA aerogels can support a 50 g weight without crush, indicating a good mechanical performance (compression strength above 1.9 MPa). The aerogels prepared from low-concentration (0.15%/0.15% and 0.15%/0.30%) dispersions are not strong enough to resist the compression but are pressed into cakes without breakage. Taking the absorption and mechanical properties into consideration, the aerogels prepared from 0.25%/0.50% (CRG/PVA) dispersion is chosen as the best material in the following investigations.

Adsorption kinetics and isotherms

To detect the adsorption mechanism of NR and IC on the CRG/PVA aerogel, the adsorption kinetics were

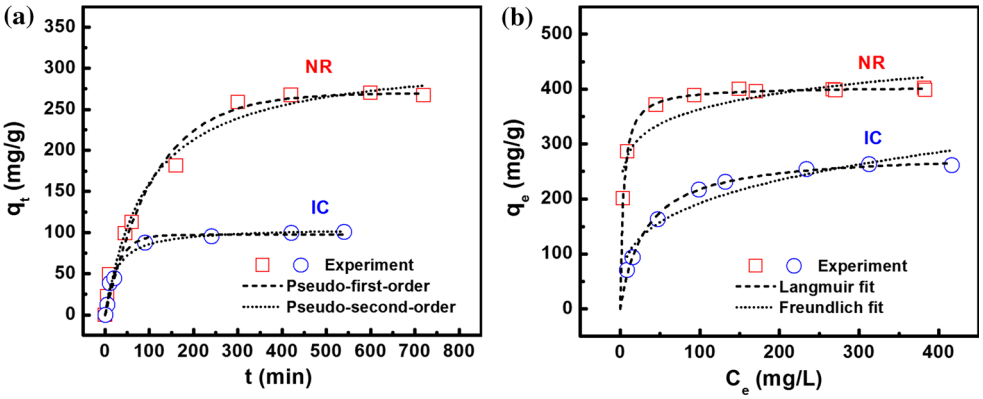

Figure 5 Adsorption kinetics (**a**) and isotherms (**b**) of NR and IC. The *symbols* present measured data, and the curves are fitted as indicated.

investigated and pseudo-first- and pseudo-second-order models [60, 61]

$$q_t = q_e\left(1 - e^{-k_1 t}\right) \tag{3}$$

$$q_t = q_e\left(1 - \frac{1}{1 + k_2 q_e t}\right) \tag{4}$$

are used to fit the experimental data (Fig. 5a). Here q_e and q_t (mg/g) are amounts of dye molecules adsorbed onto adsorbents at equilibrium and at time t (min), respectively, and k_1 (min^{-1}) and k_2 (g mg^{-1} min^{-1}) are rate constants. The fitted kinetics parameters are listed in Table S1. It is shown that the pseudo-second-order model is more applicable to describe the adsorption process, suggesting an adsorption dominated by sharing or exchanging electrons between adsorbent and adsorbate [9, 61], which is in agreement with most reports about graphene-based absorbents [20].

Figure 5b shows adsorption isotherms of NR and IC. The data are fitted by Langmuir model [62] and Freundlich model [63]

$$q_e = \frac{q_m b C_e}{1 + b C_e} \tag{5}$$

$$q_e = K C_e^{1/n} \tag{6}$$

respectively. Here, q_m is maximum adsorption capacity, b is Langmuir constant associated with binding energy, and K and n are empirical Freundlich constants representing adsorption capacity and intensity, respectively. Parameters of isotherm models are presented in Table S2. The higher correlation coefficient ($R^2 > 0.995$) of fitting by the Langmuir model indicates a monolayer coverage adsorption mechanism. The fitted q_m (NR) is 404.4 mg/g, being higher than that of many other common adsorbents, such as activated carbon (285.7 mg/g) [64], multi-walled carbon nanotube (20.5 mg/g) [13], sulfonic graphene//Fe_3O_4 (216.8 mg/g) [65], chitosan and chitin/SiO_2 hydrogel (306.1 mg/g) [66], and chitin/GO composite (165.0 mg/g) [67]. The q_m (IC) is estimated as 284.8 mg/g, being higher than that for many known adsorbents such as nut shell (1.1 mg/g) [68], maize cob carbon (150.6 mg/g) [69], halloysite nanotube (54.8 mg/g) [70], polyaniline (99.0 mg/g) [71], poly(*N*,*N*-diethylamino ethyl methacrylate) hydrogel (100.0 mg/g) [72], and PVA/SiO_2 nanofiber (266.8 mg/g) [73]. The high q_m toward NR and IC indicates that the CRG/PVA aerogel could be used as an exceptionally high-capability absorbent toward both cationic and anionic dyes, overcoming the deficiency of traditional absorbents which usually can only remove one type of organic dyes, depending on charge properties. The higher q_m of NR than IC is ascribed to the additional effect of electrostatic attraction that favors the adsorption of NR. Moreover, the absorption capabilities are superior to many known absorbents being able to absorb both cationic and anionic dyes [59, 74–80].

It is worth mentioning that the q_m (NR) of pure CRG aerogel and PVA aerogel is 706.67 mg/g and 87.40 mg/g, respectively, and the corresponding q_m (IC) is 577.59 mg/g and 67.70 mg/g, respectively, as shown in Fig. S5 and Table S3 and S4. Taking into account the mass ratio of CRG, the use efficiency of CRG in the CRG/PVA aerogel is much higher than the CRG aerogel, revealing that PVA not only brings mechanical strength and reusability but also enhances the intrinsic adsorption capability of CRG. This is crucial for cost cutting and practical applications of graphene-based adsorbents.

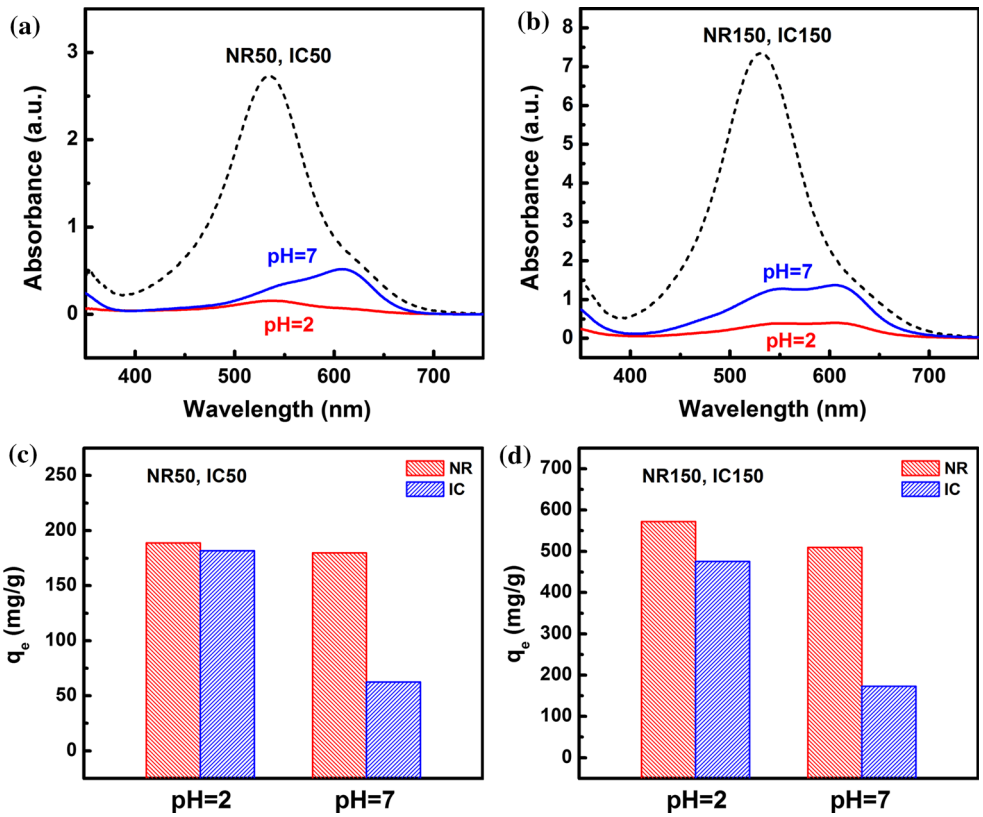

Figure 6 UV–Vis spectra of NR/IC mixture solutions [**a** C_0(IC) = C_0(NR) = 50 mg/L; **b** C_0(IC) = C_0(NR) = 150 mg/L] before (*dotted line*) and after (*solid line*) adsorption at pH = 2 and 7, and (**c**, **d**) the corresponding q_e.

Synergetic effect in binary dye solution

Considering that several kinds of dyes often coexist in wastewater in practical applications, the adsorption properties of adsorbents toward mixed dyes are of vital importance. The adsorption in IC/NR binary solutions with different pH and initial dye concentrations was investigated. Figure 6 shows UV–Vis spectra of the solutions [C_0(IC) = C_0(NR) = 50 mg/L in A, and C_0(IC) = C_0(NR) = 150 mg/L in B] before and after adsorption for 24 h using the CRG/PVA aerogel. After adsorption, the UV–Vis absorbance of dyes decreases remarkably and low pH favors the decoloration of mixed dyes. The q_e is demonstrated in Fig. 6c and d. As shown in Fig. 2, lower pH favors the adsorption of IC in single dye solution due to the shielding of electrostatic repulsion. This mechanism is applicable in the binary dye solution, too. On the other hand, higher pH no longer promotes the adsorption of NR in mixed dye solutions, which is contrary to the case of single dye solution. It seems that more IC molecules adsorbed on the CRG/PVA aerogel at pH = 2 can improve the adsorption capability of NR, pointing to an exceptional synergetic effect for NR and IC adsorption. Similar synergistic effects were observed in Congo red/rhodamine B binary system absorbed by modified yeast [81].

Given that the specific surface area of aerogel is limited, effective usage of the surface of well-dispersed CRG is responsible for the dramatically increased adsorption capability. As illustrated in Scheme 2, if only a single kind of dye is adsorbed on CRG in the CRG/PVA aerogel, the dense coverage is inhibited due to electrostatic repulsion between dye molecules charged with the same charge. In this case, there is unoccupied space among adsorbates. When two oppositely charged dyes coexist, they could be adsorbed by alternative and close arrangement to make an effective use of surface area of CRG nanosheets, yielding a much high total adsorption capability.

An important manifestation of this synergetic effect is that the total adsorption capability in mixed dye solutions (>1000 mg/g) is much higher than that in single dye solutions (<400 mg/g). The q_e removing mixed dyes is higher than that (<890 mg/g) of most

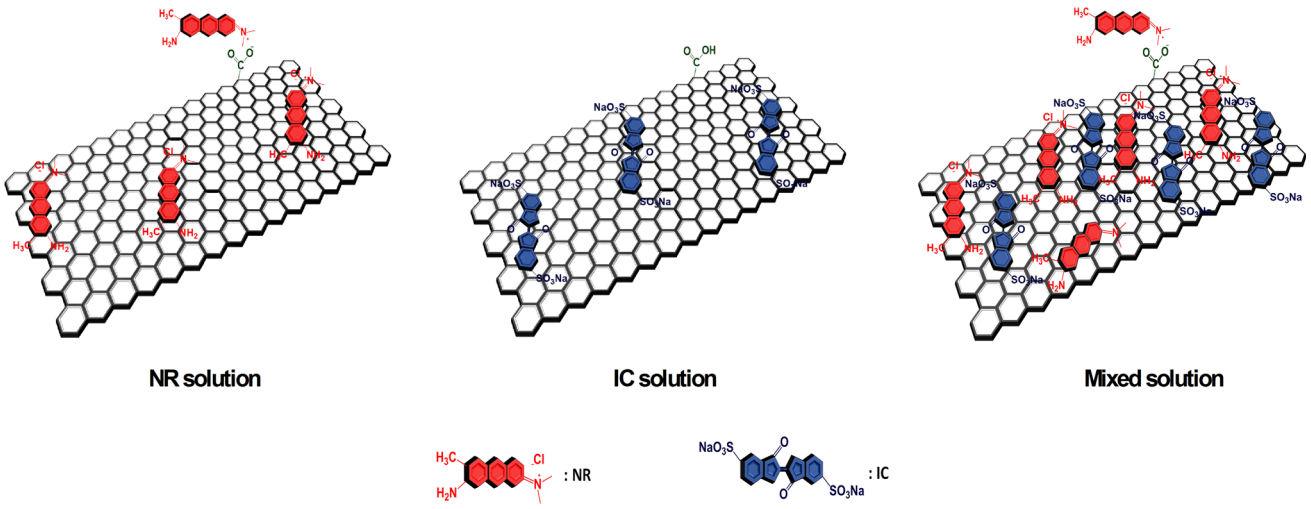

Scheme 2 Illustration of the adsorption process in single and mixed solutions.

known absorbents [82–85], making the CRG/PVA aerogel an advanced adsorbent in water treatment. Even more noteworthy is that the upper limit of total adsorption capability of the CRG/PVA aerogel in mixed dye solutions is not reached at C_0 (IC) = C_0(NR) = 150 mg/L. The huge potential of this special synergetic effect in practical applications is very attractive and deserves further investigation in later work.

Recycle performance

The recycle performance of adsorbents is important in cost cutting and practical applications. The CRG/PVA aerogels are extremely stabile in water, being able to keep their shapes well instead of shrinking or crushing (Fig. S6 in Online Resource 1). Moreover, the swollen aerogels can totally recover after compression in water (Online Resource 2) and can be regenerated by simply freeze drying again, insuring the feasibility of recycling.

NR and IC solutions of C_0 = 30 mg/L were chosen to conduct the regeneration experiment of the CRG/PVA aerogels. By washing with alcohol and 0.1M NaOH solution, respectively, the aerogels after adsorbing NR and IC can be easily regenerated and used to adsorb the dyes again. As shown in Fig. 7, after five cycles, E_r(NR) decreases slightly from almost 100% to ca. 95% and E_r(IC) from 86 to 78%. The slight decrease in adsorption capability is mainly ascribed to the small mass loss of aerogel during regeneration. These results indicate that the CRG/PVA aerogel can be regenerated easily and regarded

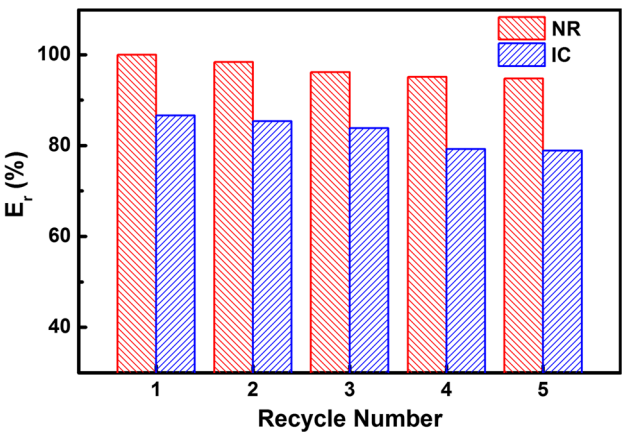

Figure 7 Removal efficiency of NR and IC after repeated adsorption–desorption cycles at C_0 = 30 mg/L.

as a reusable absorbent. But there still remains a defect that the regeneration via re-freeze drying is kind of tedious. Introduction of chemical cross-linking is a facile strategy for further improvement in dimension and performance stabilities of the aerogel, which needs further elaboration in future work.

Universality of adsorption performance

As aforementioned, the CRG/PVA aerogels adsorb both cationic NR and anionic IC mainly through π–π interaction mechanism. Raman spectrum (Fig. 8) is used to prove this mechanism. After adsorbing NR and IC, the G band of CRG in the aerogels shifts from 1595 to 1590 and 1587 cm^{-1}, respectively. In another word, both NR and IC show an electron-donating effect and cause softening of the G band [86]. As NR

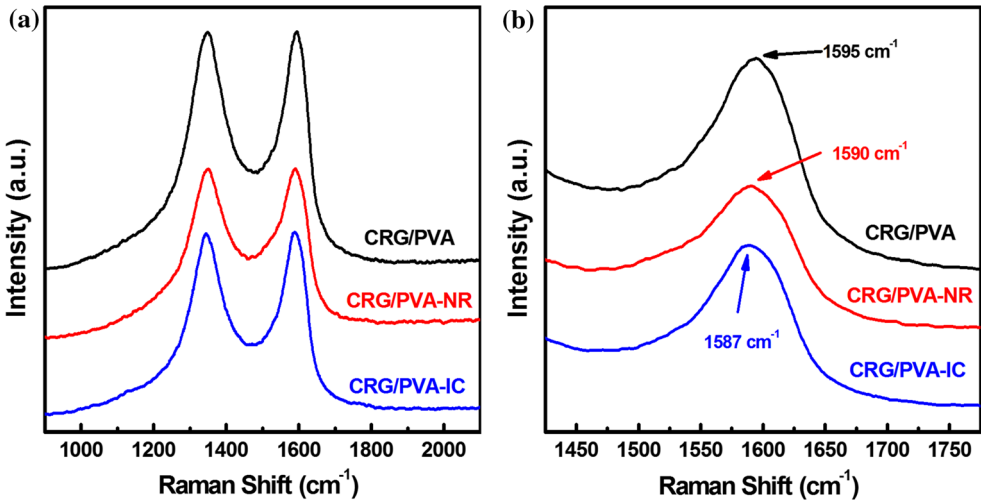

Figure 8 Raman spectra (**a**) and details about the G band (**b**) of aerogels before (fresh CRG/PVA) and after absorbing NR (CRG/PVA-NR) or IC (CRG/PVA-IC).

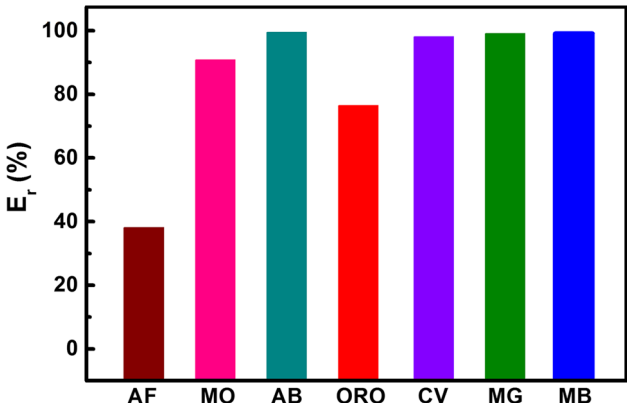

Figure 9 Removal efficiency of several anionic and cationic dyes at $C_0 = 30$ mg/L.

and IC carry opposite charges, their similar electron-donating effects confirm that the major absorption mechanism is the π–π interactions between CRG nanosheets and dye molecules [87, 88].

The major role of π–π interaction makes the aerogel to be applied as a broad-spectrum adsorbent to remove other organic dyes with aromatic structures. The adsorption ability of the aerogels toward several other anionic, nonionic and cationic dyes was investigated. Figure 9 shows E_r of the aerogels toward anionic dyes acid fuchsin (AF), methyl orange (MO) and amido black 10B (AB), nonionic dye oil red O (ORO), and cationic dyes crystal violet (CV), methylene green (MG), and MB. Chemical structures of all these dyes are shown in Scheme S1 in Online Resource 1. Absorption was performed at pH = 2 for anionic dyes and pH = 7 for nonionic and cationic dyes. Most of the dyes with $C_0 = 30$ mg/L can be almost completely removed ($E_r > 90\%$) except for anionic AF and nonionic ORO. The relatively low E_r of AF and ORO is probably due to the distortion of plane structure resulting from the steric hindrance of neighboring groups and the rotation of single bonds, which hinders the coverage and adsorption of dye molecules on the CRG surface. In another word, the conjugate plane structure is crucial for adsorption of dyes by the CRG/PVA aerogels. As almost all dyestuffs contain heterocyclic or aromatic structures [89, 90], the CRG/PVA aerogels can thus be regarded as a broad-spectrum adsorbent toward a family of organic pollutants with conjugated plane structures.

Conclusions

The CRG/PVA porous aerogels exhibit good strength, high capability, and good recycle stability for absorption of a wide kind of aromatically structured ionic and nonionic dyes via mainly π–π interaction. The total adsorption amount (>1000 mg/g) in dye mixture solutions is even higher than that of single dye solution due to the synergetic effect between oppositely charged dyes. The aerogels demonstrate absorption performance surpassing the most reported adsorbents and the highest capability toward absorption of mixture dyes, demonstrating the potential to be used as a kind of high-efficiency, reusable, and broad-spectrum adsorbents for organic dyes.

Acknowledgements

This work was supported by the National Natural Science Foundation of Zhejiang Province (Grant No.

R14E030003), the National Natural Science Foundation of China (Grant Nos. 51573157, 51333004, and 51373149), and the Major Projects of Science and Technology Plan of Guizhou Province (Grant No. (2013) 6016).

Compliance with ethical standards

Conflicts of interest The author declares no conflict of interest.

Electronic supplementary material: The online version of this article (doi:10.1007/s10853-017-0818-y) contains supplementary material, which is available to authorized users.

References

[1] Petrie B, Barden R, Kasprzyk-Hordern B (2015) A review on emerging contaminants in wastewaters and the environment: current knowledge, understudied areas and recommendations for future monitoring. Water Res 72:3. doi:10.1016/j.watres.2014.08.053

[2] Liu X, Yan L, Yin W et al (2014) A magnetic graphene hybrid functionalized with beta-cyclodextrins for fast and efficient removal of organic dyes. J Mater Chem A 2:12296. doi:10.1039/c4ta00753k

[3] Wan Q, Liu MY, Xie YL et al (2017) Facile and highly efficient fabrication of graphene oxide-based polymer nanocomposites through mussel-inspired chemistry and their environmental pollutant removal application. J Mater Sci 52:504. doi:10.1007/s10853-016-0349-y

[4] Salleh MAM, Mahmoud DK, Karim WAWA, Idris A (2011) Cationic and anionic dye adsorption by agricultural solid wastes: a comprehensive review. Desalination 280:1. doi:10.1016/j.desal.2011.07.019

[5] Qu X, Alvarez PJJ, Li Q (2013) Applications of nanotechnology in water and wastewater treatment. Water Res 47:3931. doi:10.1016/j.watres.2012.09.058

[6] Chen A, Li Y, Yu Y et al (2016) Synthesis of mesoporous carbon nanospheres for highly efficient adsorption of bulky dye molecules. J Mater Sci 51:7016. doi:10.1007/s10853-016-9991-7

[7] Liu X, Zhou Y, Nie W, Song L, Chen P (2015) Fabrication of hydrogel of hydroxypropyl cellulose (HPC) composited with graphene oxide and its application for methylene blue removal. J Mater Sci 50:6113. doi:10.1007/s10853-015-9166-y

[8] Liu S, Chen D, Zheng J et al (2015) The sensitive and selective adsorption of aromatic compounds with highly crosslinked polymer nanoparticles. Nanoscale 7:16943. doi:10.1039/c5nr04624f

[9] Yan JJ, Huang YP, Miao YE, Tjiu WW, Liu TX (2015) Polydopamine-coated electrospun poly(vinyl alcohol)/poly(acrylic acid) membranes as efficient dye adsorbent with good recyclability. J Hazard Mater 283:730. doi:10.1016/j.jhazmat.2014.10.040

[10] Gad HMH, Daifullah AE-HAM (2007) Impact of surface chemistry on the removal of indigo carmine dye using apricot stone active carbon. Adsorpt Sci Technol 25:327. doi:10.1260/026361707783432588

[11] Lv W, Du M, Ye W, Zheng Q (2015) The formation mechanism of layered double hydroxide nanoscrolls by facile trinal-phase hydrothermal treatment and their adsorption properties. J Mater Chem A 3:23395. doi:10.1039/c5ta05218a

[12] Gil A, Assis FCC, Albeniz S, Korili SA (2011) Removal of dyes from wastewaters by adsorption on pillared clays. Chem Eng J 168:1032. doi:10.1016/j.cej.2011.01.078

[13] Gong JL, Wang B, Zeng GM et al (2009) Removal of cationic dyes from aqueous solution using magnetic multi-wall carbon nanotube nanocomposite as adsorbent. J Hazard Mater 164:1517. doi:10.1016/j.jhazmat.2008.09.072

[14] Yusuf M, Elfghi FM, Zaidi SA, Abdullah EC, Khan MA (2015) Applications of graphene and its derivatives as an adsorbent for heavy metal and dye removal: a systematic and comprehensive overview. RSC Adv 5:50392. doi:10.1039/C5RA07223A

[15] Zhao GX, Jiang L, He YD et al (2011) Sulfonated graphene for persistent aromatic pollutant management. Adv Mater 23:3959. doi:10.1002/adma.201101007

[16] Wu Q, Feng C, Wang C, Wang Z (2013) A facile one-pot solvothermal method to produce superparamagnetic graphene-Fe3O4 nanocomposite and its application in the removal of dye from aqueous solution. Colloids Surf B 101:210. doi:10.1016/j.colsurfb.2012.05.036

[17] Yu JG, Yu LY, Yang H et al (2015) Graphene nanosheets as novel adsorbents in adsorption, preconcentration and removal of gases, organic compounds and metal ions. Sci Total Environ 502:70. doi:10.1016/j.scitotenv.2014.08.077

[18] Parmar KR, Patel I, Basha S, Murthy ZVP (2014) Synthesis of acetone reduced graphene oxide/Fe3O4 composite through simple and efficient chemical reduction of exfoliated graphene oxide for removal of dye from aqueous solution. J Mater Sci 49:6772. doi:10.1007/s10853-014-8378-x

[19] Xue Z, Zhao S, Zhao Z, Li P, Gao J (2016) Thermodynamics of dye adsorption on electrochemically exfoliated graphene. J Mater Sci 51:4928. doi:10.1007/s10853-016-9798-6

[20] Chowdhury S, Balasubramanian R (2014) Recent advances in the use of graphene-family nanoadsorbents for removal of

toxic pollutants from wastewater. Adv Colloid Interface Sci 204:35. doi:10.1016/j.cis.2013.12.005

[21] Sharma VK, McDonald TJ, Kim H, Garg VK (2015) Magnetic graphene-carbon nanotube iron nanocomposites as adsorbents and antibacterial agents for water purification. Adv Colloid Interface Sci 225:229. doi:10.1016/j.cis.2015.10.006

[22] Wang H, Yuan X, Zeng G et al (2015) Three dimensional graphene based materials: synthesis and applications from energy storage and conversion to electrochemical sensor and environmental remediation. Adv Colloid Interface Sci 221:41. doi:10.1016/j.cis.2015.04.005

[23] Zuo L, Zhang Y, Zhang L, Miao Y-E, Fan W, Liu T (2015) Polymer/carbon-based hybrid aerogels: preparation, properties and applications. Materials 8:6806. doi:10.3390/ma8105343

[24] Shen Y, Fang Q, Chen B (2015) Environmental applications of three-dimensional graphene-based macrostructures: adsorption, transformation, and detection. Environ Sci Technol 49:67. doi:10.1021/es504421y

[25] Liu F, Chung S, Oh G, Seo TS (2012) Three-dimensional graphene oxide nanostructure for fast and efficient water-soluble dye removal. ACS Appl Mater Int 4:922. doi:10.1021/am201590z

[26] Gao HC, Sun YM, Zhou JJ, Xu R, Duan HW (2013) Mussel-inspired synthesis of polydopamine-functionalized graphene hydrogel as reusable adsorbents for water purification. ACS Appl Mater Int 5:425. doi:10.1021/am302500v

[27] Sui Z-Y, Cui Y, Zhu J-H, Han B-H (2013) Preparation of three-dimensional graphene oxide-polyethylenimine porous materials as dye and gas adsorbents. ACS Appl Mater Int 5:9172. doi:10.1021/am402661t

[28] Xu Y, Wu Q, Sun Y, Bai H, Shi G (2010) Three-Dimensional self-assembly of graphene oxide and DNA into multifunctional hydrogels. ACS Nano 4:7358. doi:10.1021/nn1027104

[29] Bai S, Shen X, Zhong X et al (2012) One-pot solvothermal preparation of magnetic reduced graphene oxide-ferrite hybrids for organic dye removal. Carbon 50:2337. doi:10.1016/j.carbon.2012.01.057

[30] Kim H, Kang SO, Park S, Park HS (2015) Adsorption isotherms and kinetics of cationic and anionic dyes on three-dimensional reduced graphene oxide macrostructure. J Ind Eng Chem 21:1191. doi:10.1016/j.jiec.2014.05.033

[31] Cheng J-S, Du J, Zhu W (2012) Facile synthesis of three-dimensional chitosan–graphene mesostructures for reactive black 5 removal. Carbohydr Polym 88:61. doi:10.1016/j.carbpol.2011.11.065

[32] Xiao J, Lv W, Xie Z, Tan Y, Song Y, Zheng Q (2016) Environmentally friendly reduced graphene oxide as a broad-spectrum adsorbent for anionic and cationic dyes via π–π interactions. J Mater Chem A 4:12126. doi:10.1039/C6TA04119A

[33] Hummers WS, Offeman RE (1958) Preparation of graphitic oxide. J Am Chem Soc 80:1339. doi:10.1021/ja01539a017

[34] Zheng QF, Javadi A, Sabo R, Cai ZY, Gong SQ (2013) Polyvinyl alcohol (PVA)-cellulose nanofibril (CNF)-multi-walled carbon nanotube (MWCNT) hybrid organic aerogels with superior mechanical properties. RSC Adv 3:20816. doi:10.1039/c3ra42321b

[35] Zhang L, Wang Z, Xu C et al (2011) High strength graphene oxide/polyvinyl alcohol composite hydrogels. J Mater Chem 21:10399. doi:10.1039/c0jm04043f

[36] Ye M, Mohanty P, Ghosh G (2014) Morphology and properties of poly vinyl alcohol (PVA) scaffolds: impact of process variables. Mater Sci Eng, C 42:289. doi:10.1016/j.msec.2014.05.029

[37] Tan Y, Song Y, Zheng Q (2012) Hydrogen bonding-driven rheological modulation of chemically reduced graphene oxide/poly(vinyl alcohol) suspensions and its application in electrospinning. Nanoscale 4:6997. doi:10.1039/c2nr32160b

[38] Peng L, Xu Z, Liu Z et al (2015) An iron-based green approach to 1-h production of single-layer graphene oxide. Nat Commun. doi:10.1038/ncomms6716

[39] Xu Y, Sheng K, Li C, Shi G (2010) Self-assembled graphene hydrogel via a one-step hydrothermal process. ACS Nano 4:4324. doi:10.1021/nn101187z

[40] Kim S, Azuma Y, Kuwahara Y, Ogata T, Kurihara S (2015) Preparation of graphene oxide/polyvinyl alcohol microcomposites and their thermal conducting properties. Mater Lett 139:224. doi:10.1016/j.matlet.2014.10.093

[41] Xue R, Xin X, Wang L et al (2015) A systematic study of the effect of molecular weights of polyvinyl alcohol on polyvinyl alcohol-graphene oxide composite hydrogels. PCCP 17:5431. doi:10.1039/c4cp05766j

[42] Victor-Roman S, Simon-Herrero C, Romero A, Gracia I, Luis Valverde J, Sanchez-Silva L (2015) CNF-reinforced polymer aerogels: influence of the synthesis variables and economic evaluation. Chem Eng J 262:691. doi:10.1016/j.cej.2014.10.026

[43] Alhwaige AA, Herbert MM, Alhassan SM, Ishida H, Qutubuddin S, Schiraldi DA (2016) Laponite/multigraphene hybrid-reinforced poly(vinyl alcohol) aerogels. Polymer 91:180. doi:10.1016/j.polymer.2016.03.077

[44] Zhai T, Zheng Q, Cai Z, Turng L-S, Xia H, Gong S (2015) Poly(vinyl alcohol)/cellulose nanofibril hybrid aerogels with an aligned microtubular porous structure and their composites with polydimethylsiloxane. ACS Appl Mater Interfaces 7:7436. doi:10.1021/acsami.5b01679

[45] Wang Y-T, Liao S-F, Shang K et al (2015) Efficient approach to improving the flame retardancy of poly(vinyl

alcohol)/clay aerogels: incorporating piperazine-modified ammonium polyphosphate. ACS Appl Mater Interfaces 7:1780

[46] Shen P, Zhao H-B, Huang W, Chen H-B (2016) Poly(vinyl alcohol)/clay aerogel composites with enhanced flame retardancy. Rsc Adv 6:109809. doi:10.1039/C6RA21689G

[47] Zheng Q, Cai Z, Gong S (2014) Green synthesis of polyvinyl alcohol (PVA)-cellulose nanofibril (CNF) hybrid aerogels and their use as superabsorbents. J Mater Chem A 2:3110. doi:10.1039/c3ta14642a

[48] Fernandez-Merino MJ, Guardia L, Paredes JI et al (2010) Vitamin C Is an ideal substitute for hydrazine in the reduction of graphene oxide suspensions. J Phys Chem C 114:6426. doi:10.1021/jp100603h

[49] Liang J, Huang Y, Zhang L et al (2009) Molecular-level dispersion of graphene into poly(vinyl alcohol) and effective reinforcement of their nanocomposites. Adv Funct Mater 19:2297. doi:10.1002/adfm.200801776

[50] Wang Y, Shi ZX, Yin J (2011) Facile synthesis of soluble graphene via a green reduction of graphene oxide in tea solution and its biocomposites. ACS Appl Mater Int 3:1127. doi:10.1021/am1012613

[51] Bian Q, Tian H, Wang Y et al (2015) Effect of graphene oxide on the structure and properties of poly(vinyl alcohol) composite films. Polym Sci Ser A 57:836. doi:10.1134/s0965545x15060048

[52] Ali ZI, Ali FA, Hosam AM (2009) Effect of electron beam irradiation on the structural properties of PVA/V2O5 xerogel. Spectroc Acta Pt A-Molec Biomolec Spectr 72:868. doi:10.1016/j.saa.2008.12.013

[53] Mansur HS, Sadahira CM, Souza AN, Mansur AAP (2008) FTIR spectroscopy characterization of poly (vinyl alcohol) hydrogel with different hydrolysis degree and chemically crosslinked with glutaraldehyde. Mater Sci Eng C 28:539. doi:10.1016/j.msec.2007.10.088

[54] Tuinstra F, Koenig JL (1970) Raman spectrum of graphite. J Chem Phys 53:1126. doi:10.1063/1.1674108

[55] Stankovich S, Dikin DA, Piner RD et al (2007) Synthesis of graphene-based nanosheets via chemical reduction of exfoliated graphite oxide. Carbon 45:1558. doi:10.1016/j.carbon.2007.02.034

[56] Kundu A, Layek RK, Kuila A, Nandi AK (2012) Highly fluorescent graphene oxide-poly(vinyl alcohol) hybrid: an effective material for specific Au3 + Ion sensors. ACS Appl Mater Int 4:5576. doi:10.1021/am301467z

[57] Chen DZ, Li LD, Guo L (2011) An environment-friendly preparation of reduced graphene oxide nanosheets via amino acid. Nanotechnology. doi:10.1088/0957-4484/22/32/325601

[58] Zhou Q, Gong W, Xie C et al (2011) Removal of Neutral Red from aqueous solution by adsorption on spent cottonseed hull substrate. J Hazard Mater 185:502. doi:10.1016/j.jhazmat.2010.09.029

[59] Ramesha GK, Vijaya Kumara A, Muralidhara HB, Sampath S (2011) Graphene and graphene oxide as effective adsorbents toward anionic and cationic dyes. J Colloid Interface Sci 61:270. doi:10.1016/j.jcis.2011.05.050

[60] Lagergren S (1898) Zur theorie der sogenannten adsorption geloster stoffe. Kungliga Svenska Vetenskapsakademiens Handlingar 24:1

[61] Ho YS, McKay G (1999) Pseudo-second order model for sorption processes. Process Biochem 34:451. doi:10.1016/s0032-9592(98)00112-5

[62] Langmuir I (1918) THE adsorption of gases on plane surfaces of glass, mica and platinum. J Am Chem Soc 40:1361. doi:10.1021/ja02242a004

[63] Freundlich HMF (1906) Concerning adsorption in solutions. Z Phys Chem 57A:385

[64] Zhang J, Shi QQ, Zhang CL, Xu JT, Zhai B, Zhang B (2008) Adsorption of Neutral Red onto Mn-impregnated activated carbons prepared from Typha orientalis. Bioresour Technol 99:8974. doi:10.1016/j.biortech.2008.05.018

[65] Wang S, Wei J, Lv S, Guo Z, Jiang F (2013) Removal of organic dyes in environmental water onto magnetic-sulfonic graphene nanocomposite. CLEAN-Soil Air Water 41:992. doi:10.1002/clen.201200460

[66] Copello GJ, Mebert AM, Raineri M, Pesenti MP, Diaz LE (2011) Removal of dyes from water using chitosan hydrogel/SiO2 and chitin hydrogel/SiO2 hybrid materials obtained by the sol-gel method. J Hazard Mater 186:932. doi:10.1016/j.jhazmat.2010.11.097

[67] Gonzalez JA, Villanueva ME, Piehl LL, Copello GJ (2015) Development of a chitin/graphene oxide hybrid composite for the removal of pollutant dyes: adsorption and desorption study. Chem Eng J 280:41. doi:10.1016/j.cej.2015.05.112

[68] de Oliveira Brito SM, Andrade HMC, Soares LF, de Azevedo RP (2010) Brazil nut shells as a new biosorbent to remove methylene blue and indigo carmine from aqueous solutions. J Hazard Mater 174:84. doi:10.1016/j.jhazmat.2009.09.020

[69] Zhang J, Zhang P, Zhang S, Zhou Q (2014) Comparative study on the adsorption of tartrazine and indigo carmine onto Maize Cob Carbon. Sep Sci Technol 49:877. doi:10.1080/01496395.2013.863340

[70] Yu L, Wang H, Zhang Y, Zhang B, Liu J (2016) Recent advances in halloysite nanotube derived composites for water treatment. Environ Sci Nano 3:28. doi:10.1039/C5EN00149H

[71] Yasar M, Deligoz H, Guclu G (2011) Removal of indigo carmine and Pb(II) Ion from aqueous solution by polyaniline. Polym-Plast Technol Eng 50:882. doi:10.1080/03602559.2011.551978

[72] Sari MM (2010) Removal of acidic indigo carmine textile dye from aqueous solutions using radiation induced cationic hydrogels. Water Sci Technol 61:2097. doi:10.2166/wst.2010.158

[73] Li M, Wang H, Wu S, Li F, Zhi P (2012) Adsorption of hazardous dyes indigo carmine and acid red on nanofiber membranes. RSC Adv 2:900. doi:10.1039/c1ra00546d

[74] Vimonses V, Lei S, Jin B, Chow CWK, Saint C (2009) Kinetic study and equilibrium isotherm analysis of Congo Red adsorption by clay materials. Chem Eng J 148:354. doi:10.1016/j.cej.2008.09.009

[75] Song W, Gao B, Xu X et al (2016) Adsorption–desorption behavior of magnetic amine/Fe3O4 functionalized biopolymer resin towards anionic dyes from wastewater. Bioresour Technol 210:123. doi:10.1016/j.biortech.2016.01.078

[76] Deng J-H, Zhang X-R, Zeng G-M, Gong J-L, Niu Q-Y, Liang J (2013) Simultaneous removal of Cd(II) and ionic dyes from aqueous solution using magnetic graphene oxide nanocomposite as an adsorbent. Chem Eng J 226:189. doi:10.1016/j.cej.2013.04.045

[77] Fan L, Luo C, Li X, Lu F, Qiu H, Sun M (2012) Fabrication of novel magnetic chitosan grafted with graphene oxide to enhance adsorption properties for methyl blue. J Hazard Mater 215–216:272. doi:10.1016/j.jhazmat.2012.02.068

[78] Zhao J, Ren W, Cheng H-M (2012) Graphene sponge for efficient and repeatable adsorption and desorption of water contaminations. J Mater Chem 22:20197. doi:10.1039/C2JM34128J

[79] Geng Z, Lin Y, Yu X et al (2012) Highly efficient dye adsorption and removal: a functional hybrid of reduced graphene oxide-Fe3O4 nanoparticles as an easily regenerative adsorbent. J Mater Chem 22:3527. doi:10.1039/C2JM15544C

[80] Sui Z, Meng Q, Zhang X, Ma R, Cao B (2012) Green synthesis of carbon nanotube-graphene hybrid aerogels and their use as versatile agents for water purification. J Mater Chem 22:8767. doi:10.1039/C2JM00055E

[81] Yu J-x, Cai X-l, Feng L-y et al (2015) Synergistic and competitive adsorption of cationic and anionic dyes on polymer modified yeast prepared at room temperature. J Taiwan Inst Chem Eng 57:98. doi:10.1016/j.jtice.2015.05.018

[82] Yu J-x, Zhu J, Feng L-y, Chi R-a (2015) Simultaneous removal of cationic and anionic dyes by the mixed sorbent of magnetic and non-magnetic modified sugarcane bagasse. J Colloid Interface Sci 451:153. doi:10.1016/j.jcis.2015.04.009

[83] Mahmoodi NM, Ghobadi J (2015) Extended isotherm and kinetics of binary system dye removal using carbon nanotube from wastewater. Desalin Water Treat 54:2777. doi:10.1080/19443994.2014.903525

[84] Eftekhari S, Habibi-Yangjeh A, Sohrabnezhad S (2010) Application of AlMCM-41 for competitive adsorption of methylene blue and rhodamine B: thermodynamic and kinetic studies. J Hazard Mater 178:349. doi:10.1016/j.jhazmat.2010.01.086

[85] Turabik M (2008) Adsorption of basic dyes from single and binary component systems onto bentonite: simultaneous analysis of Basic Red 46 and Basic Yellow 28 by first order derivative spectrophotometric analysis method. J Hazard Mater 158:52. doi:10.1016/j.jhazmat.2008.01.033

[86] Das B, Voggu R, Rout CS, Rao CNR (2008) Changes in the electronic structure and properties of graphene induced by molecular charge-transfer. Chem Commun. doi:10.1039/b808955h

[87] Sharma P, Hussain N, Borah DJ, Das MR (2013) Kinetics and adsorption behavior of the methyl blue at the graphene oxide/reduced graphene oxide nanosheet-water interface: a comparative study. J Chem Eng Data 58:3477. doi:10.1021/je400743r

[88] Wu T, Cai X, Tan S, Li H, Liu J, Yang W (2011) Adsorption characteristics of acrylonitrile, p-toluenesulfonic acid, 1-naphthalenesulfonic acid and methyl blue on graphene in aqueous solutions. Chem Eng J 173:144. doi:10.1016/j.cej.2011.07.050

[89] O'Neill C, Hawkes FR, Hawkes DL, Lourenco ND, Pinheiro HM, Delee W (1999) Colour in textile effluents–sources, measurement, discharge consents and simulation: a review. J Chem Technol Biotechnol 74:1009. doi:10.1002/(sici)1097-4660(199911)74:11<1009:aid-jctb153>3.0.co;2-n

[90] Fu YZ, Viraraghavan T (2001) Fungal decolorization of dye wastewaters: a review. Bioresour Technol 79:251. doi:10.1016/s0960-8524(01)00028-1